Supporting Information

Kolhar et al. 10.1073/pnas.1308345110

SI Text

Image Analysis for Particle Counting. The number of particles was estimated from fluorescent images of the attached particles. The images were processed via ImageJ using rolling ball background subtraction. The number of attached particles was counted from multiple images from three independent experiments. Each bright spot in the image was counted as one particle. The main advantage of this method is that only particles are counted and there is limited interference from background fluorescence. A second advantage is that this method is far less sensitive to microscope settings such as laser intensity, exposure time, inherent differences in particle fluorescence for different shapes, and image focus, because bright spots are what are counted. This method also counts single particles or aggregated particles as one entity and eliminates bias due to aggregation. The major downside of this method is that the number of particles may be inaccurate because aggregates or particles very close to each other cannot be differentiated easily.

Model for Nanoparticle–Cell Membrane Binding. ***Model description.*** Adhesion of an antibody-displaying nanoparticle (*NP*) on a surface may be described as a reversible reaction in which the nanoparticle reacts with a surface receptor (*R*) to yield surface-bound nanoparticle (*bNP*) (1):

$$NP + R \longleftrightarrow bNP. \quad \textbf{[S1]}$$

The rate of forward reaction is k_f and the rate of reverse reaction is k_r. At equilibrium, the relationship between the concentrations of bound and free nanoparticles may be described as follows:

$$\frac{[bNP]}{[NP]} = \frac{k_f}{k_r}[R]. \quad \textbf{[S2]}$$

In the presence of fluid flow, the rate of detachment is accelerated because of shear-induced detachment and may be described by the following equation (2):

$$k_r = k_r^0 exp\left(\frac{\lambda f}{k_B T}\right), \quad \textbf{[S3]}$$

where k_r^0 is the reaction rate in the absence of shear, λ is the critical separation distance between the nanoparticle and membrane at which the antibody–antigen bond is broken, f is the fluid-induced detachment force experienced by each antibody–receptor bond, k_B is the Boltzmann constant, and T is temperature. Substituting Eq. **S3** into Eq. **S2** gives the following expression for bound nanoparticles:

$$K_b = \frac{[bNP]}{[NP]} = \left(\frac{k_f}{k_r^0}\right) exp\left(\frac{-\lambda f}{k_B T}\right)[R], \quad \textbf{[S4]}$$

where K_b is the surface partition coefficient of nanoparticles due to binding defined as the ratio of bound to free nanoparticles. The ratio $\left(\frac{k_f}{k_r^0}\right)$ may be related to the free energy of binding of nanoparticles under static conditions, $\mathbf{\Delta} G^0$, as follows:

$$\left(\frac{k_f}{k_r^0}\right) = exp\left(\frac{-\mathbf{\Delta} G^0}{k_B T}\right). \quad \textbf{[S5]}$$

Combining Eqs. **S4** and **S5** yields the following equation to describe surface binding of nanoparticles:

$$K_b = exp\left(\frac{-\mathbf{\Delta} G^0}{k_B T}\right) exp\left(\frac{-\lambda f}{k_B T}\right)[R]. \quad \textbf{[S6]}$$

Free energy of particle binding may be described in terms of the enthalpic and entropic contributions as follows:

$$\mathbf{\Delta} G^0 = \mathbf{\Delta} H^0 - T\mathbf{\Delta} S. \quad \textbf{[S7]}$$

Combining Eqs. **S6** and **S7** yields the following equation for K_b:

$$K_b = [R] exp - \left(\frac{\lambda f + \mathbf{\Delta} H^0 - T\mathbf{\Delta} S}{k_B T}\right). \quad \textbf{[S8]}$$

Contribution of shear forces. For an ellipsoidal particle with a major axis, b, and minor axis, a, the force, f, can be related to particle shape and shear rate using the following equation (3):

$$f = \frac{\mathbf{6}\pi\mu \dot{U} b \delta\sigma}{mA_c}, \quad \textbf{[S9]}$$

where μ is the liquid viscosity, $\dot{U}$ is the wall shear rate, δ is the closest distance between the nanoparticle and the surface, m is the surface density of antibodies, A_c is the area of the nanoparticles that is engaged in forming antibody–receptor bonds, and σ is a geometric factor that is only a function of the aspect ratio (3). Substituting $b = az$, where z is the aspect ratio, Eq. **S9** may be rewritten as follows:

$$f = \frac{\mathbf{6}\pi\mu \dot{U} a \delta z \sigma}{mA_c}. \quad \textbf{[S10]}$$

Contribution of enthalpy. The enthalpy of particle binding can be related to the enthalpy of forming each receptor–ligand bond, Δh, and the number of bonds engaged per particle, $N = mA_C$, as follows:

$$\mathbf{\Delta} H^0 = \Delta \boldsymbol{h} N = \Delta \boldsymbol{h} m A_C. \quad \textbf{[S11]}$$

Contribution of entropy. Binding of nanoparticles leads to a loss of entropy (4). The change in entropy associated with particle binding arises from the loss of translational, $\mathbf{\Delta} S_T$, and rotational freedom, $\mathbf{\Delta} S_R$ (5). The contribution of rotational entropy loss can be calculated based on the loss of accessible volume for the particle in the bound and free states (5):

$$\mathbf{\Delta} S = \mathbf{\Delta} S_R + \mathbf{\Delta} S_T = k_B \ln\left(\frac{\mathbf{4}\pi ab}{A_C}\frac{\mathbf{\Delta}\omega}{\mathbf{8}\pi^2}\right) + k_B \ln\left(\frac{V_b}{V}\right), \quad \textbf{[S12]}$$

where $\mathbf{\Delta}\omega$ is the rotational volume available for the nanoparticle, V_b is the volume available for a particle in the bound state, and V is the volume available for the particle in the free state. Combining Eqs. **S8** and **S10**–**S12** yields the following expression for K_b:

$$K_b = [R] exp\left[\frac{-\mathbf{6}\pi\mu \dot{U} a \lambda\sigma}{k_B T m}\frac{\delta z}{A_C} - \frac{\Delta h m}{k_B T}A_C + \ln\left(\frac{a^2}{2\pi}\frac{\Delta\omega z}{A_C}\right) + \ln\left(\frac{V_b}{V}\right)\right] \quad \textbf{[S13]}$$

Dependence of binding on parameters. Eq. **S13** relates K_b to the size, shape, and surface chemistry of nanoparticles. The first term in the

equation describes the contribution of shear forces on particle attachment.K_b decreases with increasing shear stress ($\mu\dot{U}$) and particle size, a. The particle aspect ratio affects the contribution of shear-induced detachment in several ways; the force exerted by the shear stress is proportional to the ratio of the aspect ratio, z, and contact area, A_c. The particle–membrane contact area, A_c, in turn may depend on the aspect ratio. Elongated particles likely will make a larger contact with the membrane compared with contact by spherical particles owing to the engagement of more bonds. If a direct relationship between A_c and z is assumed, then the ratio $\frac{z}{A_c}$ becomes independent of the aspect ratio. On the other hand, if the contact area of elongated particles does not increase proportionately with the aspect ratio, $\frac{z}{A_c}$ likely will increase with the increasing aspect ratio. The precise relationship between the aspect ratio and $\frac{z}{A_c}$ may depend on several other parameters, including membrane topology and the strength of antigen–antibody interaction. The approach distance, δ, between the particle and the surface also may potentially depend on the aspect ratio; σ has been found to be a relatively weak function of z (3).

The second term represents the enthalpic contribution. This contribution depends directly on the contact area, A_c, and hence the aspect ratio, z. The third term represents the contribution arising from the loss of rotational entropy of bound nanoparticles. The loss of entropy depends on shape in several ways; the $\mathbf{\Delta}\omega$ likely will decrease with increasing aspect ratio because longer particles are more likely to be constrained compared with shorter particles. The precise relationship between $\mathbf{\Delta}\omega$ and particle shape in turn may depend on several parameters, including membrane topology and the number of engaged bonds.

The final contribution arises from the loss of translational entropy of the bound nanoparticles and depends on particle volume and its concentration in synthetic microvascular networks (SMNs) (or blood). Given that the particles used in this study possessed identical volumes regardless of the aspect ratio, this term likely does not contribute to the role of shape in binding.

Eq. **S13** may be approximated under a few simplifying assumptions to highlight the dependence of K_b on key particle parameters. Specifically, assuming $\sigma \sim 1$ and assuming that neither λ nor δ depends on shape, the relative binding of rods and spheres, K^{SHAPE}, may be given by the following equation:

$$K^{SHAPE} = \frac{K_b^{ROD}}{K_b^{SPH}} = exp\left[\frac{-\mathbf{6}\pi\mu\dot{U}a\lambda\delta}{k_BTm}\left(\frac{z}{A_C^{ROD}} - \frac{1}{A_C^{SPH}}\right) - \frac{\mathbf{\Delta}hm}{k_BT}\left(A_C^{ROD} - A_C^{SPH}\right) + \ln\left(\frac{A_C^{SPH}}{A_C^{ROD}}\frac{\mathbf{\Delta}\omega^{ROD}}{\mathbf{\Delta}\omega^{SPH}}z\right)\right], \quad \textbf{[S14]}$$

where A_C^{ROD} and A_C^{SPH} are contact areas of particles with the membrane for rods and spheres, respectively, and $\mathbf{\Delta}\omega^{ROD}$ and $\mathbf{\Delta}\omega^{SPH}$ are rotational volumes available for rod and sphere, respectively ($\mathbf{\Delta}\omega^{ROD} < \mathbf{\Delta}\omega^{SPH}$).

1. Ward MD, Hammer DA (1993) A theoretical analysis for the effect of focal contact formation on cell-substrate attachment strength. *Biophys J* 64(3):936–959.
2. Hammer DA, Lauffenburger DA (1987) A dynamical model for receptor-mediated cell adhesion to surfaces. *Biophys J* 52(3):475–487.
3. Decuzzi P, Ferrari M (2006) The adhesive strength of non-spherical particles mediated by specific interactions. *Biomaterials* 27(30):5307–5314.
4. Ben-Tal N, Honig B, Bagdassarian CK, Ben-Shaul A (2000) Association entropy in adsorption processes. *Biophys J* 79(3):1180–1187.
5. Liu J, et al. (2010) Computational model for nanocarrier binding to endothelium validated using in vivo, in vitro, and atomic force microscopy experiments. *Proc Natl Acad Sci USA* 107(38):16530–16535.

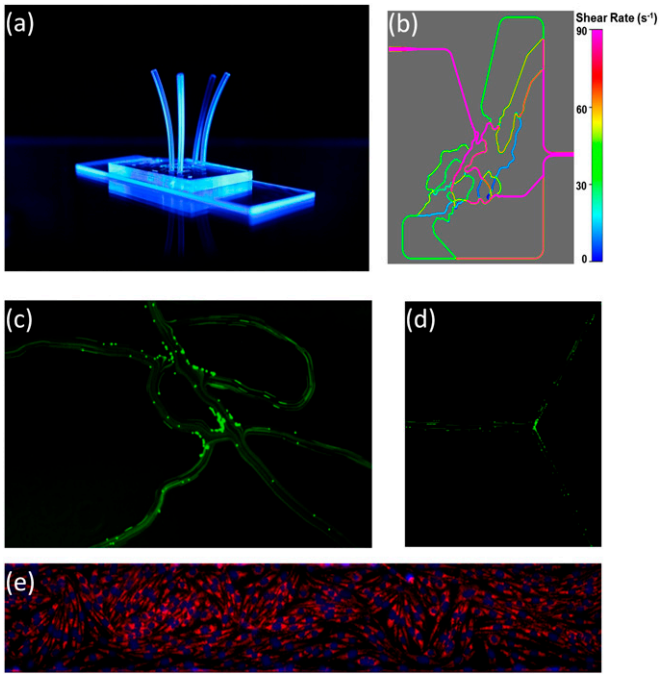

Fig. S1. Various SMN devices. (*A*) Typical SMN device fabricated on a standard microscope glass slide. The final assembled device, including tubing connecting inlet/outlet ports to the external syringe pump, is shown. (*B*) Map of shear rates in the SMN that mimic the vascular structure of the cremaster muscle, calculated as described in refs. 1 and 2. Shear rate (seconds^{-1}) maxima (magenta) and minima (blue) are represented in a heat map. (*C*) Fluorescent image of particles adhering to walls in SMNs that mimic cremaster muscle vasculature. The SMN (100 μm in width and 100 μm in height) was coated with ICAM-1, and microspheres (2 μm in diameter) were coated with anti–intracellular adhesion molecule (ICAM)-mAb. Anti–ICAM-mAb spheres were flown through SMNs at a rate of 2.5 μL/min. Microparticle accumulation is most prevalent at junctions. (*D*) Idealized SMN coated with avidin consisting of a single 120° bifurcation. Microparticles (2 μm, coated with biotin) flown at a shear rate of 240 s^{-1} also adhere in larger numbers near the bifurcation compared with the linear part of the construct. (*E*) Confluent layer of rat brain endothelial (RBE4) cells in an SMN channel. RBE4 cells are stained with Hoechst (nuclei are stained blue) and MitoTracker Red (mitochondria are stained red). For further details, see ref. 3.

1. Prabhakarpandian B, et al. (2008) Synthetic microvascular networks for quantitative analysis of particle adhesion. *Biomed Microdevices* 10(4):585–595.
2. Prabhakarpandian B, et al. (2011) Bifurcations: Focal points of particle adhesion in microvascular networks. *Microcirculation* 18(5):380–389.
3. Prabhakarpandian B, et al. (2013) SyM-BBB: A microfluidic Blood Brain Barrier model. *Lab Chip* 13(6):1093–1101.

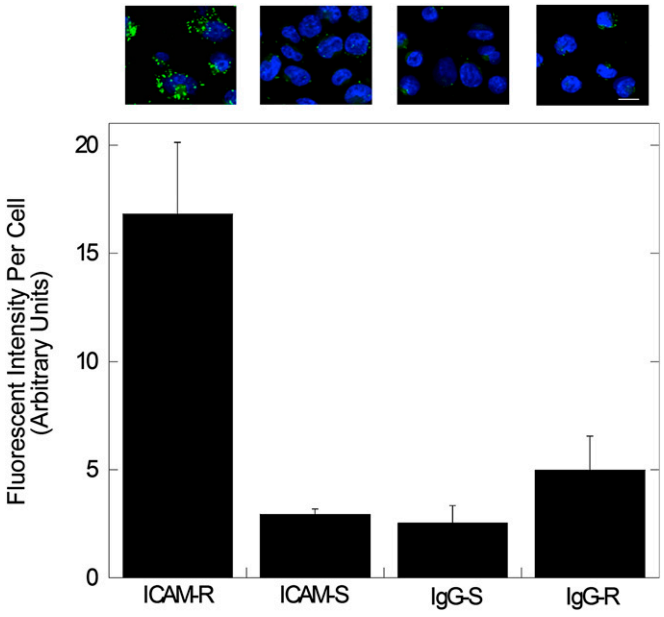

Fig. S2. Attachment of particles to endothelial cells in static cell culture. Confocal micrographs showing attachment of ICAM-mAb– or IgG-coated rods and spheres to RBE4 cells at 30 min. The bar graph shows the average fluorescence quantified in ImageJ for each particle shape and antibody. IgG-rods (IgG-R) and IgG-spheres (IgG-S) are not statistically different from each other. ICAM-rods (ICAM-R) and ICAM-spheres (ICAM-S) are statistically different from each other. Scale bar, 10 μm. Thirty cells through three independent experiments were used for image analysis.

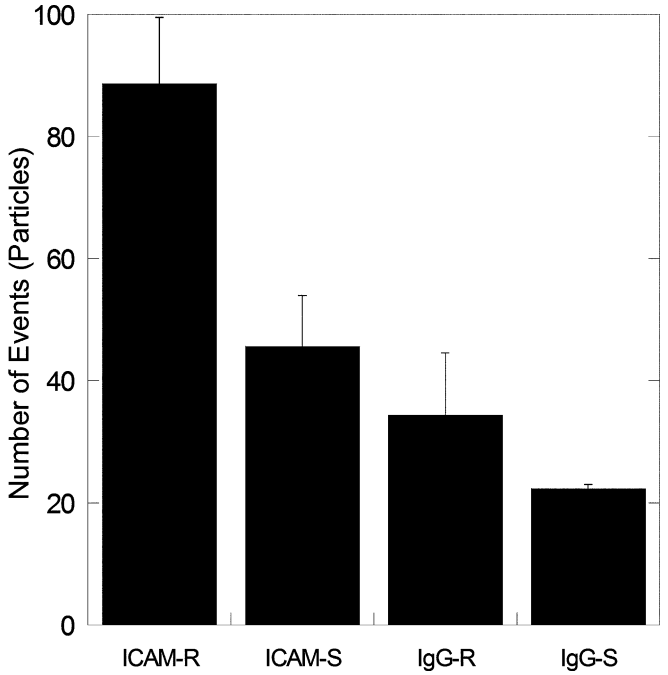

Fig. S3. Attachment of particles to endothelial cells under flow. Quantification of attachment of particles coated with IgG (spheres or rods) or anti-ICAM (spheres or rods) at 60 s^{-1} at the inlet of the device.

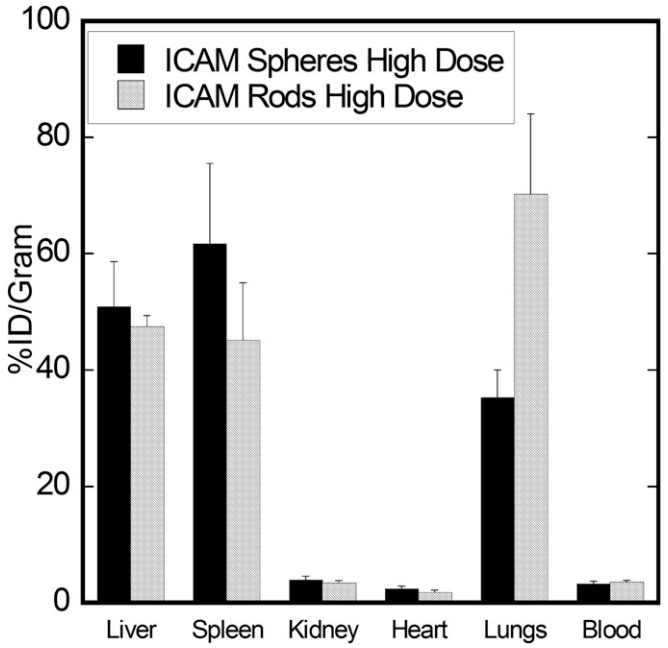

Fig. S4. In vivo biodistribution of anti-ICAM–coated particles administered in a 100-fold higher dose. The bar graph represents the percentage of injected dosage per gram of organ (%ID/gram) for anti–ICAM-mAb–coated spheres (black) and rods (hatched) for a high dose. The %ID/gram in lungs depends on the number of particles injected (n = 3–5 for all in vivo experiments).

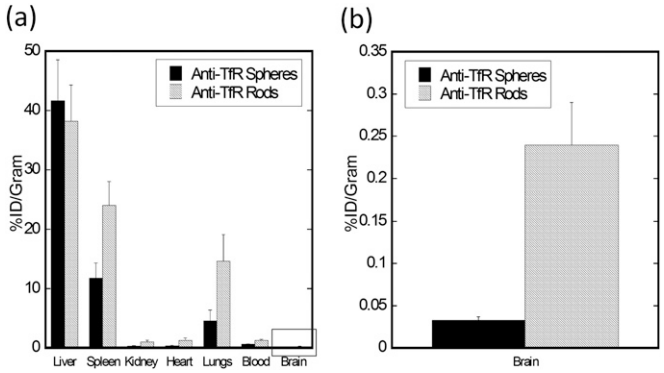

Fig. S5. In vivo biodistribution of anti-transferrin receptor (TfR)-coated particles. (*A*) Percentage of injected dosage per gram of organ (%ID/gram) for anti–TfR-mAb–coated spheres (black) and rods (hatched). (*B*) Zoomed-in view of the brain biodistribution in *A* (n = 3–5 for all in vivo experiments).

Table S1. Characterization of antibody-coated particles

Particle	Dimension(s), nm	Zeta potential, mV	Protein per 1 mg of particle, μg
IgG-spheres	205 ± 0.01, diameter	−50.9 ± 0.2	37.3 ± 4.1
IgG-rods	501 ± 43.6 × 123.6 ± 13.3	−31.2 ± 0.3	48.5 ± 2.9
ICAM-spheres	205 ± 0.01, diameter	−43.2 ± 2.1	45.53 ± 4.6
ICAM-rods	501 ± 43.6 × 123.6 ± 13.3	−23.6 ± 0.4	66.25 ± 15.5
TfR-spheres	205 ± 0.01, diameter	−48.4 ± 1.0	41.43 ± 7.8
TfR-rods	501 ± 43.6 × 123.6 ± 13.3	−30.1 ± 0.1	48.2 ± 12.4